Article:
Ai, S., Dai, R. and Long, H. orcid.org/0000-0003-1673-1193 (2020) Investigating formability enhancement in double side incremental forming by developing a new test method of tension under cyclic bending and compression. Journal of Materials Processing Technology, 275. 116349. ISSN 0924-0136

https://doi.org/10.1016/j.jmatprotec.2019.116349

Accepted Manuscript

Title: Investigating formability enhancement in double side incremental forming by developing a new test method of tension under cyclic bending and compression

Authors: Sheng Ai, Rui Dai, Hui Long

PII: S0924-0136(19)30321-8
DOI: https://doi.org/10.1016/j.jmatprotec.2019.116349
Article Number: 116349

Reference: PROTEC 116349

To appear in: *Journal of Materials Processing Technology*

Received date: 17 January 2019
Revised date: 23 July 2019
Accepted date: 28 July 2019

Please cite this article as: Ai S, Dai R, Long H, Investigating formability enhancement in double side incremental forming by developing a new test method of tension under cyclic bending and compression, *Journal of Materials Processing Tech.* (2019), https://doi.org/10.1016/j.jmatprotec.2019.116349

Investigating formability enhancement in double side incremental forming by developing a new test method of tension under cyclic bending and compression

Sheng Ai, Rui Dai, Hui Long*

Department of Mechanical Engineering, The University of Sheffield, Sheffield, UK, S1 3JD

* Corresponding author. Tel.: +44 114 222 7759

E-mail address: h.long@sheffield.ac.uk

Abstract

Incremental sheet forming (ISF), including single point incremental forming (SPIF) and double side incremental forming (DSIF), has demonstrated significantly enhanced material formability compared to traditional sheet metal forming processes. However, the material deformation mechanisms that lead to the enhanced formability in DSIF are not fully understood. In this study, a new test method, named as *Tension under Cyclic Bending and Compression (TCBC)*, has been developed to investigate four deformation modes observed in DSIF, including tension, compression, bending and cyclic loading, on the material formability enhancement. An analytical model based on the elementary plasticity theory has been developed to characterize the effect of tension, compression, bending and cyclic loading on the initiation of material plastic deformation. A TCBC rig has been manufactured and experimental tests of two aluminium alloys have been conducted by applying the Design of the Experiments to investigate the significant effects of different deformation modes on the material formability. Finite element modelling of TCBC test as well as DSIF process has also been developed to compare their plastic strain evolution and strain paths during the cyclic deformation process. The material formability has been found to be improved significantly under TCBC condition and the existence of compression loading leads to strengthened localized material plastic deformation, which contributes to the enhanced material formability and delayed fracture. The new TCBC test method developed in this study has demonstrated its potential to replace the current testing method using the DSIF process itself for material formability studies.

Key words: DSIF; formability; tension under cyclic bending and compression.

Nomenclature

σ_{φ}^{A}	Tensile stress in the longitudinal direction (MPa)
σ_t	Contact stress between the bending roller and the specimen (MPa)
σ_c	Contact stress between the compression roller and the specimen (MPa)
σ_s	Material flow stress (MPa)
r_t	Radius of the bending roller and the compression roller (mm)
w	Width of the deformed specimen (mm)

φ	Contact angle between bending roller and the specimen
t	Thickness of the specimen under deformation (mm)
ε_l	Strain in the longitudinal direction
v_t	Tensile speed (mm/s)
v_s	Stroke speed (mm/s)

1. Introduction

Incremental sheet forming (ISF) has received much research attention from the academia and the industry in the past decade due to its excellent process flexibility and enhanced material formability when compared with the conventional sheet metal forming processes. In ISF, the tools move along predesigned toolpaths and a sheet metal blank is deformed progressively into the designed geometry. Depending on the tools used in the process, ISF can be categorized into single point incremental forming (SPIF), double side incremental forming (DSIF) and two-point incremental forming (TPIF). To further improve the material formability and forming accuracy thus further extend the applicability of the ISF process, heat-assisted ISF processes have also been developed by Duflou et al. (2008) using laser beam and by Liu et al. (2016) using electrical current. A comprehensive review on the development of the ISF technology has been reported by Emmens et al. (2010) and recent development in the last decade has been reviewed by Behera et al. (2017) and Duflou et al. (2017). The process flexibility makes ISF an ideal manufacturing technology for product customization in automotive (Jeswiet and Hagan, 2001), aerospace (Rodríguez, 2006) and medical (Lu et al., 2016) applications.

The improved material formability in ISF for various materials, including steel (Fratini et al., 2004), pure titanium (Hussain et al., 2008) and alumnum alloy (Kim and Park, 2002) has been widely reported. A detailed review on ISF formability enhancement and fracture mechanisms explaining different types of fracture behaviour observed in experiments has been reported (Ai and Long, 2019). The formability improvement is attributed to the localized material deformation during the ISF process. For SPIF, the localised deformation results from a combination of tension, bending, shearing and cyclic loading effect, as shown in Figure 1(a). The effect of each deformation mode on the material formability was qualitatively analysed by the method of classic mechanics of materials (Emmens and van den Boogaard, 2009). To confirm the existence of these deformation modes and to investigate their influence on ISF process, experimental, finite element (FE) modelling and analytical techniques have been widely employed. By using a membrane analysis method, Silva et al. (2008) and Martins et al. (2008) obtained the stress distribution in the deformation zone and assessed the influence of the key process parameters of ISF, such as tool size, sheet thickness and friction. In addition, lower hydrostatic stresses were observed in ISF, in comparison with the deep drawing process. As a low hydrostatic stress delayed damage initiation and propagation due to plastic deformation, higher material formability could be achieved in ISF. To improve the membrane method, which ignored the bending effect, Fang et al. (2014) considered the bending effect explicitly in an analytical model and its effect on the stress and strain distributions was obtained. By comparing the results considered bending effect with that from the membrane models, a similar stress distribution in the meridional direction was found however the existence of bending led to a greater tensile stress on the outer surface of the ISF part without fracture. In addition, the fractography of a crack in ISF manufactured conic part confirmed the presence of bending effect. By engraving grids onto the cross-section of welded copper plates,

Jackson and Allwood (2009) observed the existence of through-thickness shear (TTS) not only in the tool movement direction but also in the direction perpendicular to the tool movement direction, in addition to tension and bending effects. The influence of TTS on the formability of materials was further investigated by Eyckens et al. (2009) using the extended Marciniak-Kuczynski (M-K) model. In contract, Lu et al. (2014) found that shearing effect resulted from friction-related factors had no significant influence on the material formability in SPIF when a tool with an oblique head was used. By comparing strain and stress distributions obtained from FE simulations, Smith et al. (2013) also confirmed the existence of tension, bending and shearing effects in SPIF process. The relative significance between these deformation modes depended on the selection of the process parameters, according to the observation of the strain distribution on the deformed parts using digital image correlation (DIC) technique, reported by Eyckens et al. (2011). In conclusion, the interactions between the multiple deformation modes played an important role in determining the material deformation behaviour thus the formability in SPIF process.

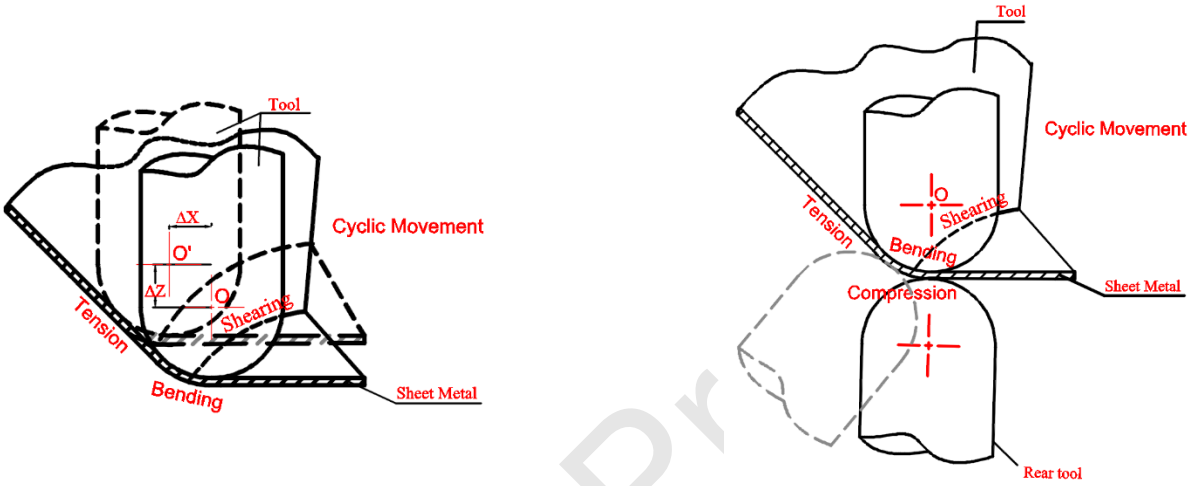

(a) (b)

Figure 1 Schematic of different deformation modes in ISF: (a) SPIF; (b) DSIF

DSIF is an improvement made to SPIF. In DSIF, an additional tool as a partial die is added on the other side of the sheet, opposite to the main tool. Greater material formability and geometric accuracy could be achieved in DSIF as well as higher process flexibility than SPIF, as reported by Smith et al. (2013) through performing comparative tests between SPIF and DSIF. In addition to the tension, bending, shearing deformation modes and cyclic loading in SPIF, a superimposed compression mode from the additional real tool was introduced in DSIF, the relative location between the rear tool and the forming tool can be adjusted, as shown in Figure 1(b).

The influence of the introduced compressive force between the main and additional tools is twofold. Firstly, it makes the contact conditions in DSIF more complex. Instead of a single bending zone in the contact area in SPIF, the contact area in DSIF can be divided into at least two single contact zones and one dual contact zone. The distribution of the contact stresses also depends on the relative location of the two tools. Secondly, the existence of compression will change the stress and strain distributions not only on the sheet surfaces but also in the sheet thickness direction. By establishing a theoretical analysis model, Lu et al. (2015) obtained the stress distribution in the contact areas. A drastic drop of stress triaxiality was found in the dual contact area in DSIF, which indicted a possible zone of local material deformation, resulting in the enhanced material formability. While in the experiment, when the compressive force from the supporting tool was

varied from 160N to 640N, an increase of forming depth of the conic shape was observed first but a decrease of the formability occurred after the compressive force was increased to 540N. The influence of the relative position of the two tools was also investigated by Lu et al. (2015). Furthermore, Smith et al. (2013) compared the SPIF with Accumulative-DSIF (ADSIF) by applying FE analysis and found that higher hydrostatic pressure and TTS contributed to higher material deformation stability in ADSIF. In addition, the additional tool added an extra contact point to the deforming sheet thus creating more bending-unbending cycles during forming the material, resulted in greater material work-hardening which further strengthened the localised deformation of the material.

In addition to the process parameters, material properties of the deforming sheet have also been proved to affect the material deformation behaviour in ISF. Fratini et al. (2004) conducted a statistical analysis of the relative importance of mechanical property related factors by using various materials including copper, steel and aluminium alloys in SPIF tests and reported that the work-hardening had the greatest effect on material formability in SPIF. Jeswiet et al. (2005) also observed difference of maximum forming angles when using ISF to produce the same geometry with different materials. While comparing the material forming limit in SPIF with that obtained from bulge test using material AA5251-O and AA1100, Ai et al. (2017) found different materials showed different fracture behaviours when the final fracture failure occurred.

However, the existence of multiple deformation modes and contact conditions prohibits a systemic evaluation of the influence of individual deformation modes on the fracture behaviour in ISF, especially in DSIF. Alternatively, simplified testing methods representing the loading conditions in ISF process allow in-depth investigations into the deformation mechanism in ISF. As mentioned above, Eyckens et al. (2009) investigated the TTS effect by performing the M-K test. Morales et al. (2009) investigated the interaction between tension and bending effects in the stretch-bending test. Furthermore, Emmens and van den Boogaard (2009) adopted the continuous bending and tension test (CBT), in which the complicated loading conditions in SPIF was simplified into a two-dimensional problem. Each deformation mode, including tension, bending and cyclic loading effect was independently investigated by varying the value of corresponding parameters. Localised deformation was observed in the tests and it was found that the actual bending radius controlled by tension force and bending depth was the most influential factor on the material formability in the CBT test.

Compared with many studies published on SPIF, the reported work on DSIF is limited. The superimposition of the compression onto the existing deformation modes in SPIF is a simple way to evaluate the contribution of the compression to the localisation of material deformation according to the Tresca yielding criterion. To simplify the analysis process, DSIF has been widely treated as SPIF with a superimposed compressive backing force. Almost all the currently published papers in DISF are focused on the compression effect on the material formability without considering individual and interactive effects from other factors. Moreover, the dual contact zone between the tools and the sheet not only changes stress and strain distributions but also the division of the contact zones, adding more complications into the analysis of DSIF. Furthermore, the influence of other process factors also contributes to the material deformation in DSIF, individually or interactively. The simplified testing methods, for example the CBT test, provide an alternative investigation method into the material deformation in ISF. However, in the CBT test, the tool

moving speed was set to be constant. The tool moving speed is a reflection of the cyclic effect in the ISF process, ignoring its variation may undermine the significance of its effect on the material deformation. Regarding to investigating the damage evolution in the material, the progressive deformation of ISF makes it difficult to directly observe the initiation and evolution of the damage in the material.

To develop a better understanding regarding the material deformation and fracture behaviour in DSIF, a new testing method, *Tension under Cyclic Bending and Compression* (TCBC), is developed in this research, with the capability beyond the CBT test. In the newly developed TCBC test, the major deformation modes in DSIF, including tension, bending and compression with cyclic loading effect can be independently controlled by adjusting corresponding testing parameters. A theoretical analysis model has been established based on the elementary theory in the dual contact zone between the tools and the specimen. Using this model, the influence of compression, bending and tension loading conditions has been analysed. In addition, the material formability under different loading conditions and process parameters has been investigated and compared with the experimental results obtained from the developed TCBC testing rig. Two types of aluminium alloys, AA5251-H22 and AA6082-T6, have been tested in the experiments where the Taguchi Design of the Experiments has been used to plan the test runs. The maximum elongation of tested specimen and the force history have been recorded for each test. Statistical analysis of the significance of tested factors has been carried out based on the recorded experimental data. To understand the material deformation history in the specimen during the TCBC test, FE modelling of the test has been developed using the FE solver Abaqus/Explicit. The evolution of stress and strain distributions during the TCBC testing process has been obtained. Combined with the FE modelling results, the material deformation behaviour during the experiment has been thoroughly analysed and evaluated.

2. Tension under cyclic bending and compression test

2.1 The concept of TCBC test

In the CBT test platform developed by Emmens and van den Boogaard (2009), the specimen was stretched in the longitudinal direction while bent at a certain depth against a cylindrical roller, which moved cyclically along the specimen length direction, thus the material deformation under tension and bending with cyclic effect could be investigated. To accommodate the superimposed compressive force from the additional tool employed in DSIF, in the newly developed TCBC test, another cylindrical roller is positioned against the bending roller to provide a compressive force from the other side of the specimen. The concept of the TCBC test is illustrated in Figure 2.

The compression roller is pressed by cylindrical springs to provide compression as well as to maintain the contact between the compression roller and the specimen. The length and stiffness of the springs can be adjusted thus the magnitude of the compression can be varied. In order to ensure the bending effect to the target zone and maintain the presence of the bending effect, the specimen is kept in position by two supported rollers positioned with a constant distance, as shown in Figure 2. All four rollers move cyclically to create a localised deformation of the target zone on the specimen along the longitudinal direction, representing the deformation characteristics in DSIF.

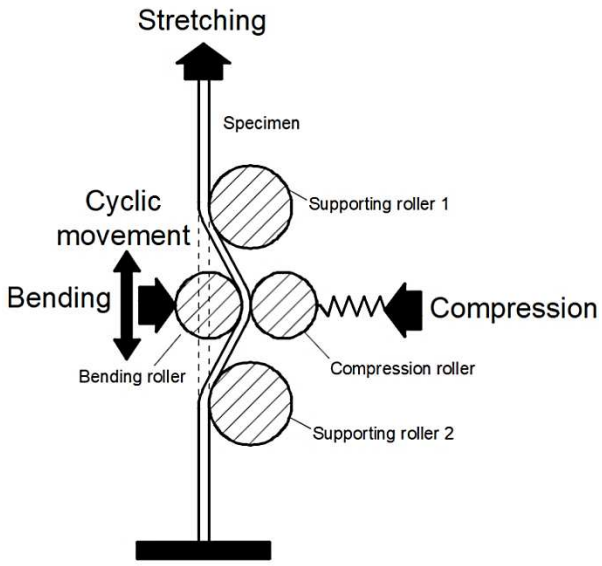

Figure 2 Schematic of the TCBC test concept considering the compressive loading in DSIF

Based on the concept of the TCBC test, a test rig has been designed and manufactured to perform the experiment. The developed rig is shown in Figure 3, consisting of two specially designed components, a loading device and motor controlling system.

Various loadings conditions can be applied onto the specimen by using the loading device. The loading device is mounted on a uniaxial tensile test platform so that its stiffness and position accuracy can be guaranteed. Both ends of the specimen are clamped and the specimen is stretched from one end by the movement of the linear screw mechanism driven by a DC motor. Bending and compression loadings onto the specimen are applied by the loading device in which two cylindrical supporting rollers as well as bending and compression rollers are positioned against each other with a gap. The specimen can be inserted through the gap and bent from below by the bending roller and compressed from above by the compression roller. Using the loading device, both the compressive force and the bending depth can be adjusted. All the rollers are designed to be free to rotate around its own axis to reduce friction. The loading device can move along a slider, which is mounted on the base of the uniaxial tensile test platform and the loading device is driven by another DC motor. On both ends of the slider, a micro switch is placed, once the loading device hits the switch, the rotating direction of the DC motor will be reversed, creating a cyclic movement of the loading device. The speed and the starting direction of both motors can be controlled by the controller.

In summary, by using the developed TCBC test rig, the stroke speed of the slider, the tensile speed, the bending depth and the compression can be independently controlled and varied in the experiment. These correspond to the effect of each deformation mode in DSIF, including cyclic effect, tension effect, bending effect and compressive effect. A load cell is installed on the left-hand side of the uniaxial tensile test platform so that the tensile force during the test can be measured and recorded.

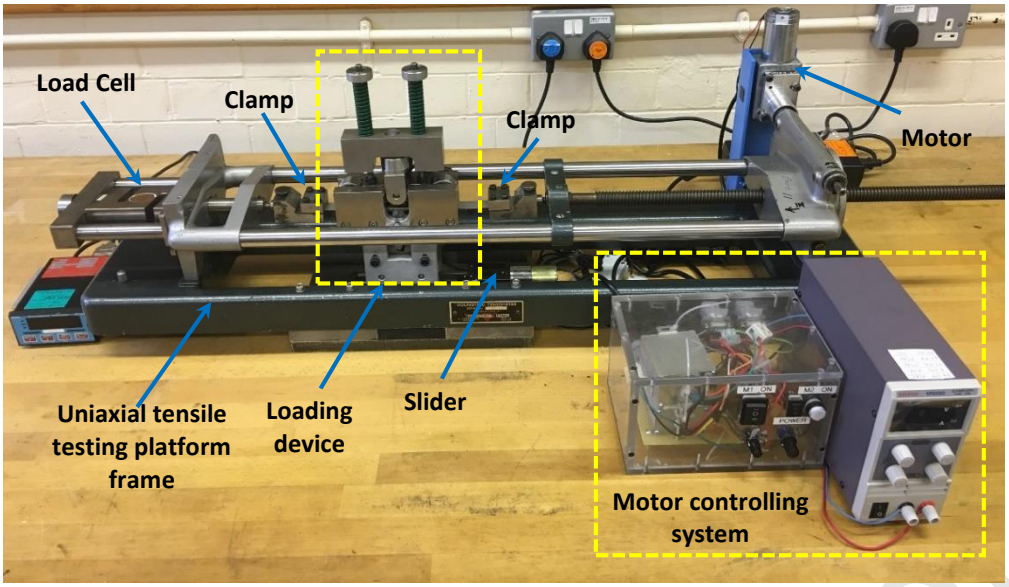

Figure 3 Key components of the TCBC test rig

2.2 Theoretical analysis of material deformation in TCBC test

Material deformation can be determined by the stress and strain states during the manufacturing process. Theoretical analysis of the targeted deformation area can provide a detailed and explicit description of the stress and strain distributions of the material under deformation, which in turn enables the formability analysis. Due to the cylindrical geometry of the rollers, the contact zone between the specimen and the bending roller is only in partial contact with the compression roller, as shown in Figure 4(a). According to the contact conditions between the rollers and the specimen, the testing region of the specimen in the TCBC test, L, can be divided into three zones, the single contact zone, the dual contact zone and the uniaxial tensile zone, as shown in Figure 4(b). For the simplicity of the theoretical model, the following assumptions are made:

- The bending depth is small so that the single contact zone is comparatively much smaller than the dual contact zone, therefor the single contact zone can be ignored;
- For a material with good ductility, the thickness reduction of the specimen upon fracture is considerably large and the specimen is thin so that the stress variation across the thickness direction can be ignored (Ai et al., 2017);
- The contact stresses in the contact zone on both sides of the specimen are uniformly distributed.

To obtain the stress distribution of the deformed area, an infinitely small element is extracted from the dual contact zone of the specimen, Figure 4(a). The dimension of the element in the lateral direction is equal to the width of the specimen at the deformation point while the dimension in the longitudinal direction is assumed to be infinitely small. The dimensions to define the element and the stress components applied onto the element are shown in Figure 4(c). From the force equilibrium of the element in the radial direction of the curved specimen, the following equation can be obtained:

$$\left[\sigma_\varphi \cdot (t+dt)\cdot(w+dw)+\left(\sigma_\varphi+d\sigma_\varphi\right)\cdot t\cdot w\right]\cdot\sin\frac{d\varphi}{2}+\sigma_c\cdot(r_t+t)\cdot d\varphi \cdot\frac{2w+dw}{2}=\sigma_t\cdot r_t\cdot d\varphi\cdot\frac{2w+dw}{2} \tag{1}$$

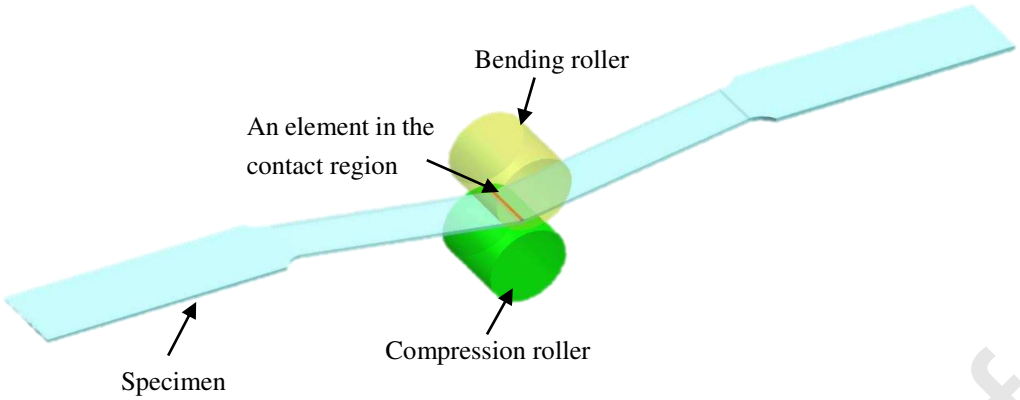

(a)

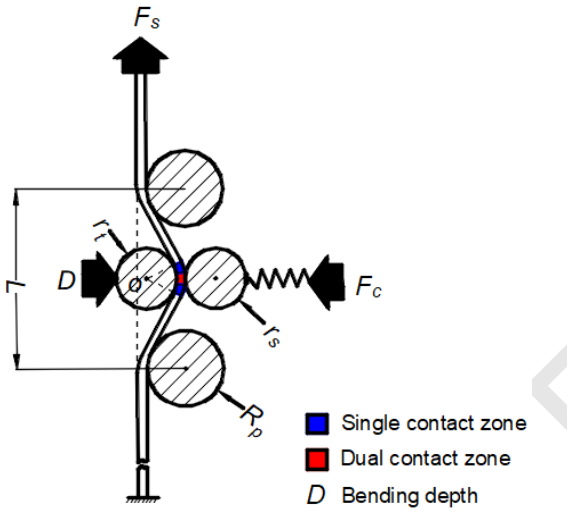

(b)

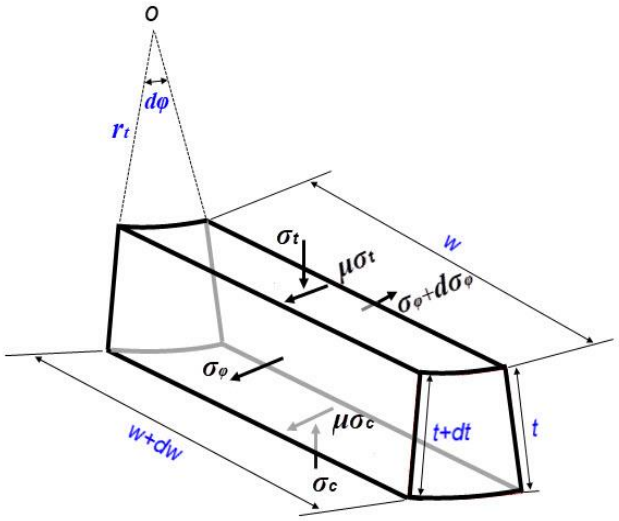

(c)

Figure 4 Schematic of the simplified theoretical analysis model: (a) The selected element in contact region for analysis; (b) Schematic of the contact conditions in TCBC test; (c) Stress components applied onto the selected element.

By ignoring higher-order terms, Equation (1) is reduced to:

$$\sigma_\varphi \cdot (2t \cdot w + t \cdot dw + w \cdot dt) + d\sigma_\varphi \cdot t \cdot w = [\sigma_t \cdot r_t - \sigma_c \cdot (r_t + t)] \cdot (2w + dw) \quad (2)$$

According to the volume conservation law in plastic deformation,

$$\frac{dw}{w} + \frac{dt}{t} + d\varepsilon_l = 0 \quad (3)$$

Substituting Equation (3) into Equation (2), it can be shown that,

$$\sigma_\varphi \cdot (2 - d\varepsilon_l) + d\sigma_\varphi = \left[\sigma_t \cdot \frac{r_t}{t} - \sigma_c \cdot \left(\frac{r_t}{t} + 1\right)\right] \cdot \left(2 + \frac{dw}{w}\right) \quad (4)$$

The radius of the bending roller and the compression roller of the developed TCBC rig is $r_t = 10mm$ while the thickness of the specimen is generally in the range of 1.0~1.5 mm. As a result, $\frac{r_t}{t}$ is much larger than 1 while at the same time $\frac{dw}{w}$ is infinitely small, therefore Equation (4) can be further simplified as,

$$\sigma_\varphi = (\sigma_t - \sigma_c) \cdot \frac{r_t}{t} \tag{5}$$

Combining the Tresca yielding criterion, $\sigma_\varphi + \sigma_t = \sigma_s$, with Equation (5), the relationship of the stress components of the selected element in the deformation zone can be obtained as,

$$\begin{aligned} \sigma_t &= \frac{\sigma_s + \sigma_c \cdot \frac{r_t}{t}}{1 + \frac{r_t}{t}} \\ \sigma_\varphi &= \frac{\frac{r_t}{t}}{1 + \frac{r_t}{t}} \cdot (\sigma_s - \sigma_c) \end{aligned} \tag{6}$$

Using these equations, the relationship between the normalized compressive stress $\frac{\sigma_c}{\sigma_s}$, the ratio of tool radius to the sheet thickness $\frac{r_t}{t}$ and the normalized tensile stress $\frac{\sigma_\varphi}{\sigma_s}$ can be obtained, as shown as a 3D plot in Figure 5(a) and a top view of the 3D plot in Figure 5(b).

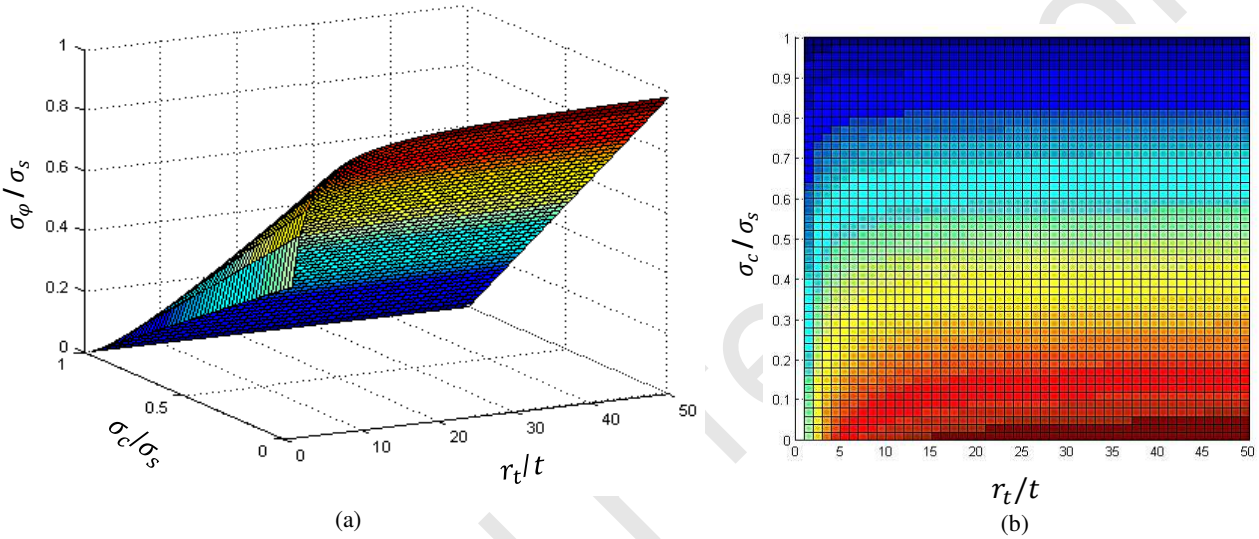

(a) (b)

Figure 5 Theoretical analysis results of the influence of the key parameters on the tensile stress

According to the results reported by Fang et al. (2014) and Emmens and van den Boogaard (2009), the fracture of the deforming sheets in SPIF process and CBT test were all caused by material tension. In addition, according to the Tresca yielding criterion and current design of the TCBC test rig, tension is essential to create localised plastic deformation. Therefore, the tensile stress in the longitudinal direction can be considered as a driving factor of the material deformation in the TCBC test. From Figure 5(a) it is evident that the higher the compressive stress is, the smaller tensile stress is required to reach the plastic deformation of the material in TCBC test. Viewing the variation of the tool radius/sheet thickness ratio in Figure 5(b), its effect on the required tensile stress for plastic deformation is less obvious. However, when the tool radius/sheet thickness ratio is less than 15, it is clear that the ratio has an effect on the tensile stress required for reaching the plastic deformation.

Bending effect is not explicitly considered in the theoretical analysis model, mainly due to neglecting the thickness effect in the deviations. However, the bending roller radius/sheet thickness ratio can still be used as an indicator of the bending effect due to the existence of the curvature of the analysed element. The effect of the bending varies depending on the magnitude of the ratio. When the radius of the bending roller becomes too large, the bending effect is minimised and the

sheet material is mainly under compression and tension. An obvious transition of the significance of the bending effect can be seen in Figure 5(b), showing the normalized tensile stress variations under varying bending radius/sheet thickness ratio and normalized compressive stress. When the bending effect is strong by using a bending roller with a smaller radius, the tensile stress required for plastic deformation is obviously smaller than that using a bending roller with a larger radius. Furthermore, when the bending effect is reduced to a certain level, the bending deformation would no longer contribute to the tensile stress reduction and the tensile stress remains almost constant.

In addition, a competition of the dominance on the material deformation also exists between the compression effect and the bending effect. As shown in Figure 5(b), when the compressive stress is comparatively small, the bending effect is more dominant, while when the compressive stress is increased, the bending effect becomes less influential.

In the developed test rig, the designed stroke speed v_s is much higher than the tensile speed v_t, the time needed for the rollers to travel through the contact zone in one loading cycle can be calculated as,

$$\Delta T = \frac{r_t \cdot \mathrm{d}\varphi}{v_s}$$

Thus the strain increment of the contact zone in this time period can be determined as,

$$\Delta\varepsilon_l = \frac{v_t \cdot \Delta T}{r_t \cdot \mathrm{d}\varphi} = \frac{v_t \cdot \Delta T}{v_s \cdot \Delta T} = \frac{v_t}{v_s} \tag{7}$$

The frictional effect due to the contact between the rollers and the specimen is ignored based on the fact that the rollers are not fixed thus free to rotate, resulted in small rolling contact friction. In the longitudinal direction of the specimen, the force equilibrium of the element can be established as,

$$\sigma_\varphi \cdot (t + dt) \cdot (w + dw) \cdot \cos\frac{d\varphi}{2} = \left(\sigma_\varphi + d\sigma_\varphi\right) \cdot t \cdot w \cdot \cos\frac{d\varphi}{2} \tag{8}$$

By simplification and combining Equation (3) and Equation (8), it can be obtained that,

$$-d\varepsilon_l = \frac{d\sigma_\varphi}{\sigma_\varphi} \tag{9}$$

It can be solved as,

$$\varepsilon_l = \ln\sigma_\varphi + C \tag{10}$$

where C is an integration constant.

Combining Equation (6), (7) and (10), it can be obtained that,

$$\ln\frac{\sigma_{\varphi n+1}}{\sigma_{\varphi n}} = \frac{v_t}{v_s} \tag{11}$$

where n is the number of deformation cycles that the material has been subjected to during ISF. From Equation (11) it can be concluded that, the higher the difference between the tensile speed and the stroke speed is, the greater difference of the tensile stresses exists between the two ends of the dual contact zone. If the speed difference is large enough, when the stroke speed v_s is considerably small or v_t is reasonably high, the TCBC loading condition will degenerate to a simple tension, therefore the material formability could not be improved. In general, a higher stroke speed and lower tensile speed will be beneficial to the formability enhancement of the material in the TCBC test.

3. The experimental investigation

3.1 Design of the Experiments

The experiment was conducted in three stages. In the first stage, in order to understand the effect of the TCBC load conditions on the material formability enhancement, the maximum elongation of materials under different combinations of the loading conditions were compared, including uniaxial simple tension, tension under cyclic compression (TCC), tension under cyclic bending (TCB). The schematic of these loading conditions are shown in Figure 6.

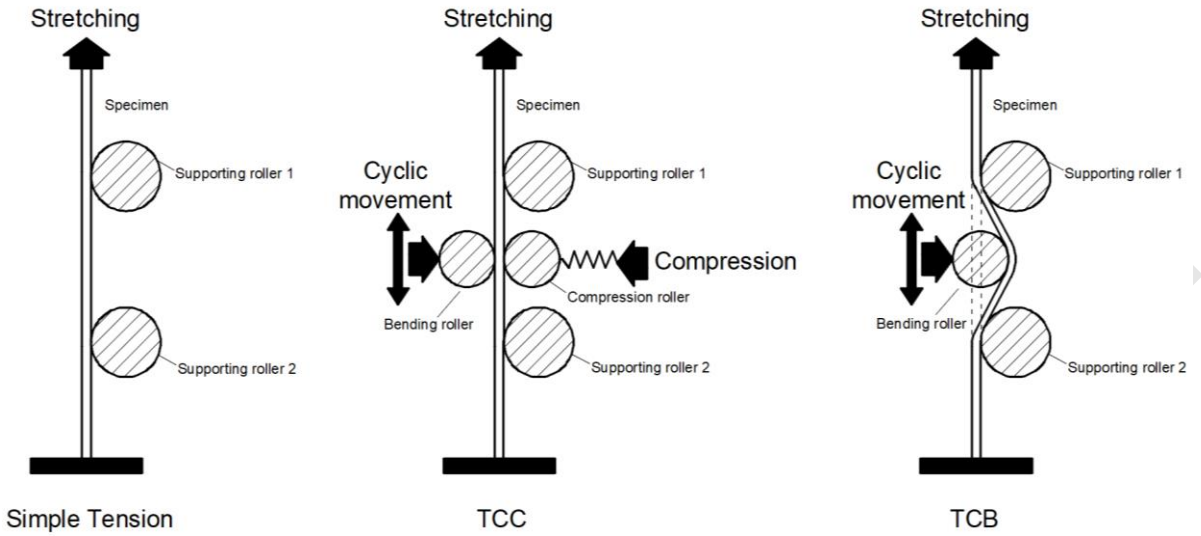

Figure 6 Schematics of different combination of loading conditions

As can be seen from Figure 2, to reflect the influence of each loading condition, five parameters can be varied during the TCBC test. These are the compressive force from the compression roller, the bending depth from the bending roller, the stroke speed of the slider, the tensile speed of the linear screw, and the specimen thickness. Other parameters of the test rig in these tests were kept the same. The maximum elongations of the specimens and displacement-force curves were measured and recorded.

To accommodate the dimensions of the test rig, a specimen based on the ASTM-E8 standard (2009) was designed, the dimensions are shown in Figure 7. Material AA5251-H22 was used in the first stage of the experiment.

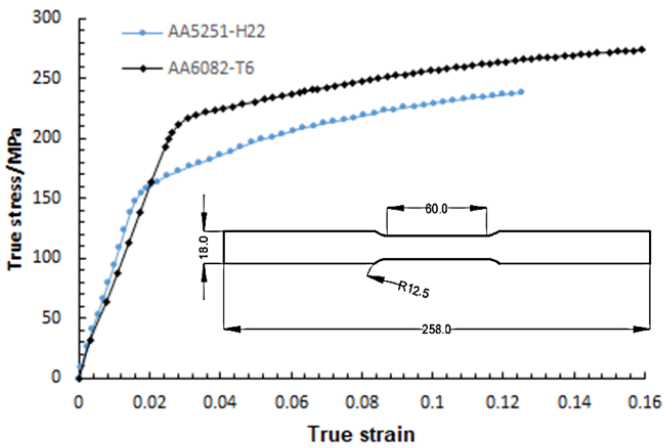

Figure 7 Flow stress curves of material AA5251-H22 and AA6082-T6 obtained from the uniaxial tensile test

In the second stage of the experiment, the effect and significance of individual parameters on the maximum elongation of the specimen in the TCBC test were investigated. The tested ranges of the parameters are shown in Table 1. The parameter variation ranges were decided by taking into consideration of the dimensions of the test rig, the characteristics of the motors and the equivalent process parameter values commonly used in ISF. In order to investigate the influence of the material properties on the formability in this stage of experiment, two types of materials with distinct flow stress properties were tested, the aluminium alloy AA5251-H22 and AA6082-T6. The flow stress curves of the two materials obtained from the uniaxial tensile tests are shown in Figure 7.

Table 1 Variation ranges of test parameters used in the second stage TCBC experiment

Tested parameters	Parameter Variation Ranges	
	AA5251-H22	AA6082-T6
Compressive force	150-900N	600-1200N
Bending depth	3-9mm	3-9mm
Stroke speed	0.5-2.5mm/s	0.5-2.5mm/s
Tensile speed	1.6-3.2mm/min	1.6-3.2mm/min
Specimen thickness	1.0, 1.2, 1.5mm	1.0, 1.5mm

Considering the number of the parameters investigated, a full factorial experiment design will be resource-and-time-consuming. To minimize the number of sets of experiment to be conducted and at the same time to ensure that the experimental results provide important insights into the interactive effects of the tested parameters, Taguchi Design of Experiments method has been applied to optimize the design of test runs. Since material properties can be reflected by several factors, for example yielding stress, work-hardening coefficient and ultimate tensile strength, the material type was not chosen to be a factor in the second stage TCBC experiment.

Table 2 Mixed-level Taguchi design of the experiments for AA5251-H22

Test number	Compressive force(N)	Bending depth (mm)	Stroke speed (mm/s)	Tensile speed (mm/min)	Thickness (mm)
1	150	3	0.5	1.6	1.0
2	150	6	1.5	2.4	1.2
3	150	9	2.5	3.2	1.5
4	300	3	0.5	2.4	1.2
5	300	6	1.5	3.2	1.5
6	300	9	2.5	1.6	1.0
7	450	3	1.5	1.6	1.5
8	450	6	2.5	2.4	1.0
9	450	9	0.5	3.2	1.2
10	600	3	2.5	3.2	1.2
11	600	6	0.5	1.6	1.5
12	600	9	1.5	2.4	1.0
13	750	3	1.5	3.2	1.0
14	750	6	2.5	1.6	1.2
15	750	9	0.5	2.4	1.5

16	900	3	2.5	2.4	1.5
17	900	6	0.5	3.2	1.0
18	900	9	1.5	1.6	1.2

Material AA5251-H22 was chosen to be the tested material in the Taguchi Design of the Experiments because of its higher sensitivity to the designed ranges of the testing parameters than that for AA6082-T6. The test of the material AA6082-T6 was conducted separately. Details of the tests of AA5251-H22 by the mixed-level Taguchi design of the experiments are shown in Table 2. A L18 orthogonal array was generated with the help of the statistical analysis software Minitab 17 (Minitab, 2014). A similar mixed-level Taguchi design of the experiments for AA6082-T6 was also created according to the levels of variations defined in Table 1.

As a useful statistical method, Taguchi Design of Experiments provides considerably robust response for a wide range of investigated parameters from a small number of experiments. However, some of the intermediate values are ignored and a trend of the effect of the parameter based on the Taguchi Design of the Experiments may only be partially correct. In ISF, bending and compression effects are considered to be the most important and the interaction of these two deformation mechanisms affects the material formability in ISF considerably. To better understand the influence of these two mechanisms, in the final stage of the experiment, additional two sets of experiments were performed. In the first set of the final stage of the experiments, the influence of the compression force was investigated by only varying the value of the compressive force. While in the second set of the final stage of the experiments, the bending depth and specimen thickness were adjusted to investigate the bending effect. Other parameters remained unchanged in both tests of the final stage of the experiments.

3.2Experimental procedures

Before each test to commence, the specimens were inserted between the rollers and bent by the bending roller in the middle of the specimens to the tested bending depth shown in Tables 1 and 2. Then the compressive force was applied by adjusting the compression springs. Both ends of the specimens were then clamped. The speed of the both motors was adjusted to the tested values and could be switched on simultaneously. The specimen was deformed and stretched until fracture occurred. The load-displacement curve during the test was measured and recorded by the load cell on the fixed end of the specimen. The maximum elongation of the specimen was also measured as an indicator of the material formability in each test. To ensure the repeatability of the test results, each set of the test was performed twice to ensure the robustness of the results and an average value of the maximum elongations obtained was calculated. If the discrepancy between the maximum elongations obtained in the first two trials exceeded 5%, a third test was conducted and the two values of similar maximum elongations was used to calculate the average value of the maximum elongation for the test.

4. Experimental test results

4.1 Comparison of tested specimens under different loading conditions

4.1.1 Maximum elongations of the tested specimens

In the first stage of the test, a comparison of the maximum elongation values between the tests has been made. During the first stage tests, the tensile speed and the stoke speed were fixed to be 2.4mm/min and 1.5mm/s respectively. The bending depth was adjusted to be 9mm and the compressive force was set to be 900N in the TCC, TCB and TCBC tests, if the parameters were applicable to each type of the tests. A comparison of the final length of the specimens after test under different loading conditions is shown in Figure 8. In the uniaxial tensile test, the averaged maximum elongation was 10.2mm, while for the TCBC test, the averaged maximum elongation almost reached 70mm. Compared to the uniaxial tension condition, TCC and TCB achieved a significant increase of the maximum elongation. The TCBC condition achieved the highest formability enhancement among all tests, in which the tested region of the specimen was elongated almost as twice as its original length.

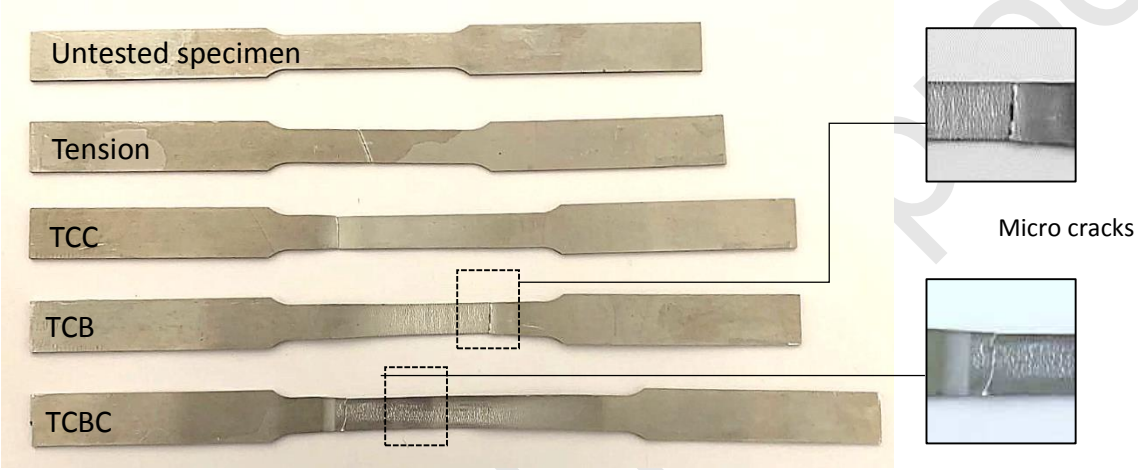

Figure 8 Elongation of tested specimens under different loading conditions

4.1.2 Fracture behaviours of the tested specimens

The fracture behaviour of the specimens was also different under different test conditions, as shown in Figure 8. In the simple uniaxial tension test, the crack occurred at an angle to the lateral direction of the specimen. While in other tests, the cracks were all parallel to the lateral direction. The difference of the crack directions was resulted from the different stress distribution in the deformation zone of the specimen induced by different loading conditions. In the simple uniaxial tension test, the whole central target zone was under uniform tensile stress and the angle of the crack direction matched the orientation of the maximum shearing stress plane. While in the TCC, TCB and TCBC tests, the introduction of compression / bending or both promoted localized plastic deformation and confined the deformation zone to a small area within or near the contact zone. As a result, the shift of the orientation of the cracks indicated a change to localised deformation in the specimen under TCC, TCB and TCBC loading conditions investigated.

In addition, multiple micro cracks can be observed on the convex surface of the specimens due to bending effect under TCB and TCBC conditions, however the concave surface shows no crack. Under simple uniaxial tension and TCC loading conditions, no evident trace of micro cracks is observed on either side of the specimens before the final fracture. This phenomenon indicates that

the effect of bending on the deformation behaviour during bending-related processes of TCB and TCBC. The existence of bending leads to higher stress triaxiality and tensile stress in the longitudinal direction of the specimen, which promote the development of micro cracks on the convex surface of the specimen. However, the existence of compression strengthens the localised deformation in the contact area of the specimen thus significantly reduces the tensile stress required for the plastic deformation. As a result, instead of undergoing a rapid evolution of the cracking, as occurred in the uniaxial tensile test, the propagation of the micro cracks is suppressed by compression in the TCBC test. The micro cracks continue existing and increasing while the deformation process progresses until the final fracture occurs.

4.1.3 Force-displacement histories of the tests

The tensile force-displacement histories recorded during the tests are shown in Figure 9. Contrary to the maximum elongation each test produced, the force needed was the highest for the simple uniaxial tension test but the lowest for the TCBC test. While for the TCC and TCB test, the tensile forces required were almost equal for the same degree of deformation.

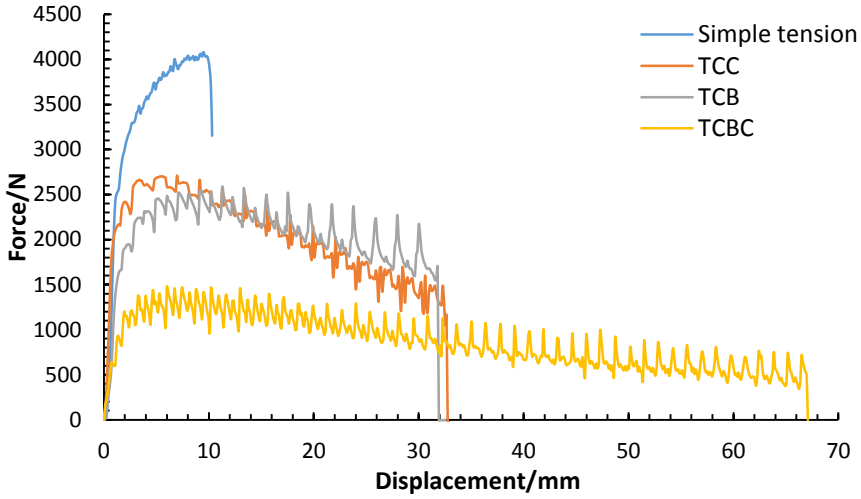

Figure 9 Displacement-force curves recorded during tests under different loading conditions

4.2 Effects of individual parameters in TCBC test

4.2.1 Significance of individual parameters

The recorded maximum elongation in each set of the experiment was regarded as the response in the Taguchi Design of the Experiments. With the help of the software Minitab 17 (Minitab, 2014), the influence of each factor on the maximum elongation in the TCBC test, representing the formability of the material, was analysed. Since only one response has been defined in the Taguchi Design of the Experiments, only signal-to-noise (S/N) ratio and means of the response could be used for the analysis of the significance of the factors. In the mean value analysis, the *p*-value is used as an indicator to determine the statistical significance of the investigated factors. For a significance level of 0.1 (confidence level of 90%) in testing AA5251-H22, the compression (*p*-value=0.045), bending depth (*p*-value=0.062) and the stroke speed (*p*-value=0.072) were the most significant factors affecting the maximum elongation, while the tension speed (*p*-value=0.105) and the specimen thickness (*p*-value=0.286) were not important. The statistical analysis result based on the experiments in this study was quite different to the observation in the CBT test reported by Emmens and van den Boogaard (2009a), in which the bending depth and tensile speed, representing the actual bending effect in SPIF, were the most important factors. While in testing AA6082-T6 in

this study, the *p*-values were all greater than 0.1, which meant none of the investigated factors was found to have a significant effect on material formability in the TCBC test at a confidence level of 90%.

4.2.2 Relative significance of individual parameters

The relative significance of the factors can be reflected based on ranking of the Delta statistics in the Taguchi method (Minitab, 2014). In this study, the focus is to maximize the elongation of the specimen. Therefore, the mean value of the maximum elongation was chosen to be the target for the analysis of relative significance of the tested factors. As shown in Figure 10, in the investigated variation ranges of the factors, all factors for both types of materials had a main effect on the means. However, it was obvious that material AA5251-H22 was far more sensitive to the variation of the five factors investigated than that of AA6082-T6. The maximum and minimum values of the averaged maximum elongation achieved in the experiment were plotted in Figure 10. The minimum difference of the mean of means for material AA5251-H22 was 14.9% and the maximum difference was 86.3%; while the maximum difference for material AA6082-T6 was only 18.9%. By comparing formability enhancement achieved by SPIF between material AA5052 and AA1100, Ai et al. (2017) concluded that a material with lower work-hardening but higher ductility was more easily influenced by the SPIF process parameters. This observation supported the findings obtained in the TCBC test in this study. A possible explanation could be that among all the deformation mechanisms, a different mechanism may dominate not just because varied process parameters, as pointed out by Eyckens et al. (2011) and by Maqbool and Bambach (2018), but also due to the difference in material properties. For a material with greater work-hardening, tension effect dominated over bending and shearing. As a result, for material AA6082-T6, the deformation behaviour was not significantly influenced by the factors applied in the TCBC test.

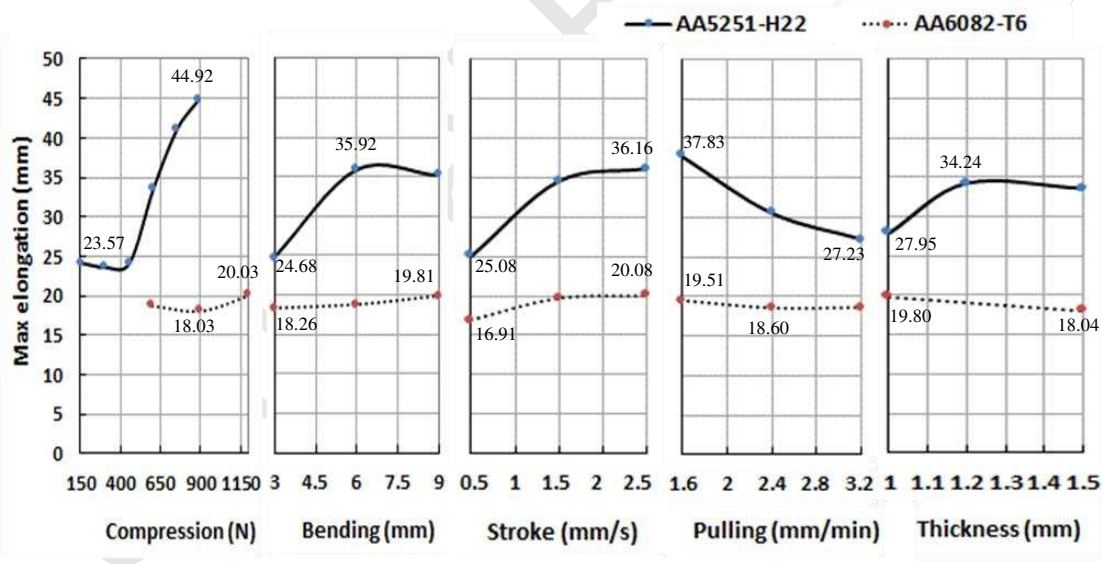

Figure 10 Main effect plot of the factors for the mean in TCBC test of AA5251-H22 and AA6082-T6

The relative significance between individual factors also varied for the same type of material. For material AA5251-H22, as shown in Figure 10, the compression showed the largest variation between all the levels, meaning the greatest effect on the maximum elongation, while bending depth was the second and stroke speed was the third most important factor. Tensile speed and specimen thickness were still the least significant factors, a similar observation with the analysis made by using the p-value analysis. For material AA6082-T6, stroke speed was the most influential factor,

and compression force was the second most important factor, while specimen thickness, bending depth and tensile speed were the lease important factors.

4.2.3 Significance of individual parameters at different levels

The slope of the lines in Figure 10 can be used to compare the relative magnitude of effect of each factor at different levels. For material AA5251-H22, for compression, no significant effect was shown between 150N and 450N while significant effect was displayed when the compression force was increased to 750N. The trend started to change from increase to decrease when the compression was further increased to 900N. For bending depth, increasing it from 3mm to 6mm produced obvious effect on the maximum elongation while when it was further increased, much less effect could be seen, this observation was the same as predicted by the theoretical analysis model presented in Section 2.2. A similar trend was also observed for the stroke speed. For the tensile speed, an obvious negative effect was found when it was increased from 1.6mm/min to 3.2mm/min. The specimen thickness also produced insignificant effect when the thickness was increased from 1.2mm to 1.5mm.

For material AA6082-T6, both bending depth and stroke speed had a positive effect on the maximum elongation through the whole investigated variation ranges of these two factors, while specimen thickness showed a slightly negative effect. Tensile speed firstly showed a slightly negative effect when increased from 1.6mm/min to 2.4mm/min, however when it was further increased to 3.2mm/min, the effect of tensile speed became minimal. Increasing the compression from 600N to 900N led to a slight reduction of the maximum elongation, while further increasing it to 1200N, an increase of the maximum elongation was observed. A similar trend of minor drop in the maximum elongation could also be observed when increasing the compression from 150N to 300N for material AA5251-H22.

4.3 Investigation into the compression and bending effect

The second stage experimental results provided evidences that the compression force and the bending depth were the most influential factors in the TCBC test for material AA5251-H22. In addition, bending effect was not only affected by the bending depth, but also by the specimen thickness. Further evaluation by the full factorial design of the experiments was conducted to investigate the effect of these two deformation modes.

4.3.1 Compression effect

In this test, all the factors were fixed except for the compression. The specimen had a thickness of 1.5mm, the bending depth was set to be 9mm, the stroke speed and the tensile speed were maintained as 1.5mm/s and 2.4mm/min respectively. A greater range of the compression varying from 150N to 1500N was investigated.

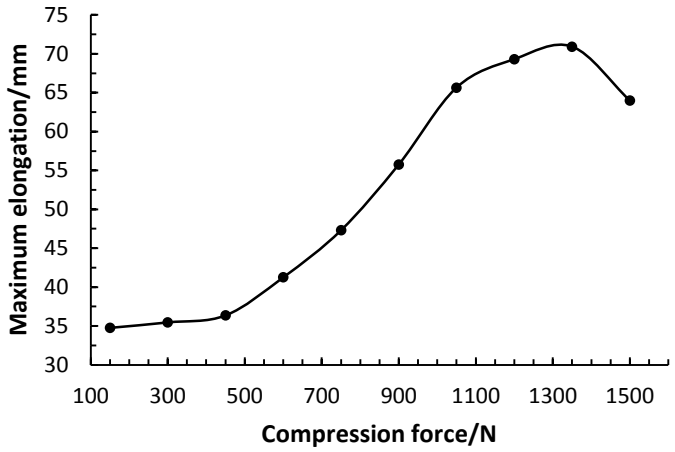

Figure 11 The influence of compression on the maximum elongation in TCBC

The relationship between different values of the compression and the obtained maximum elongations is shown in Figure 11. A different trend of the results from the Taguchi Design of the Experiments results can be observed, in which compression forces of less than 900 N were investigated. The compression force firstly had a positive effect on the maximum elongation before it reached 1300N while an adverse trend occurred when the compression force was further increased to 1500N. An explanation can be made by comparing the fracture locations of the tested specimens. In these tests, when the compression was large enough, fracture occurred at a location where the bending and compression rollers started to switch the cyclic movement direction. When the compression was moderate, the plastic deformation in the contact zone could be shared by a large area to compensate for the tension effect. However, when the compression force was large enough, the contact area yielded easily by compression and created a weak zone over a short period of time of cyclic loading. This observation corresponds to the finding from the theoretical analysis presented in Section 2.2 that the tensile speed has an adverse effect on the maximum elongation of the specimen. If the tensile speed is set to infinitely small, the whole TCBC process is transformed to a cyclic rolling process so that the deformation can be extremely large without the occurrence of fracture.

4.3.2 Bending effect

Different from the compression effect, which is only determined by the magnitude of the compression force, bending effect from a static point of view can be affected by the bending roller radius, bending depth and the specimen thickness. According to Schrader and Elshennawy (2014), the bending effect can be affected by the tool radius, blank thickness and bending angle in their study. In the TCBC test in this study, the diameter of the rollers is kept to be 10mm and the bending angle is determined by the bending depth. Therefore the bending effect in the TCBC test is affected by two factors, the thickness of the sheet blank and the bending depth. The larger the bending depth and the specimen thickness are, the greater the bending effect is.

Four sets of tests of the further experiment were conducted. In the first two sets of the tests, the compression was maintained to be 900N and the material thickness was 1.5mm. In the first set of the tests, the bending depth was varied at 0mm, 3.0mm, 6.0mm and 9.0mm respectively. In the second set of the tests, the thickness was varied to be 1.0mm, 1.2mm and 1.5mm respectively. In the last two sets of the tests, the compression was set to be zero and bending depth was set to be 9mm. The variation of the specimen thickness was the same as that in the first two sets of the

experiments. The stroke speed and the tensile speed were fixed to be 1.5mm/s and 2.4mm/min respectively. The relationship between the bending depth/specimen thickness and the maximum elongation of the specimen is shown in Figure 12. As can be seen in Figure 12(a), within the investigated variation range of the bending depth, an obvious trend of enhanced maximum elongation could be observed when the bending depth was increased, with or without the compression effect. For different specimen thicknesses, a different trend was observed when tested with or without the compression effect. As shown in Figure 12(b), when no compression force applied, increasing the specimen thickness from 1.0mm to 1.2 mm then to 1.5mm only achieved a limited increase of the maximum elongation. While when a greater compression of 900N was applied, the maximum elongation increased significantly first then dropped considerably.

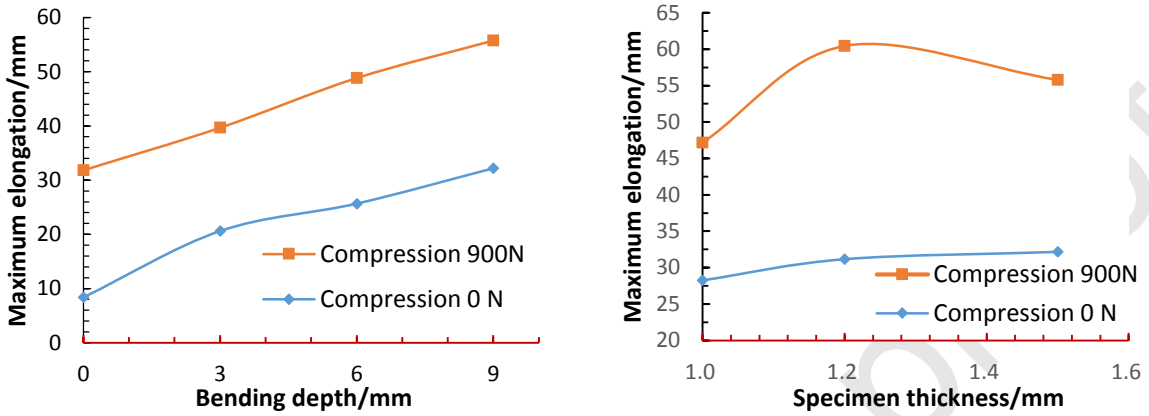

Figure 12 The maximum elongation under different compression forces with varying: (a) Bending depth; (b) Specimen thickness

5. Finite element modelling of TCBC test

Although the TCBC test has enormously simplified the analysis of the material deformation in DSIF, the developed TCBC test rig, as shown in Figure 3, does not facilitate a direct observation of the deformation history of the deformed material. Techniques such as the digital image correlation (DIC) could not be applied because the contact area was covered by the moving rollers. Laser-engraved grids on the outer surface of the specimen were used by Fang et al. (2014) to calibrate the strain distribution on the convex surface of the deformed area in SPIF. Combined with the thickness measurement, the strain distribution in three major directions could be obtained. However, in DSIF the abrasion from the contact between outer surface of the specimen and the additional tool will damage the grid. A direct experimental measurement of strains and stresses in the TCBC test by using laser-engraved grids is not feasible.

Finite element (FE) method has been proved to be both effective and efficient in investigating the material deformation history by obtaining strain and stress distributions. In this section, FE simulation models of the TCBC and TCB process were developed. Stress and strain distributions during the test process were obtained and compared. Based on the results, the material deformation and fracture behaviour in the tests were evaluated.

5.1 FE modelling of TCBC process

Considering the high non-linearity resulting from contact conditions and the large material plastic deformation, the FE modelling of the TCBC and TCB processes was performed using the Abaqus/Explicit solver. Material AA5251-H22 was used in the model. As observed in the

experiment, the material could reach much greater plastic deformation under TCBC and TCB conditions than that in the uniaxial tensile test. As a result, the plastic stress-strain curve obtained by the uniaxial tensile test is insufficient to describe material deformation in the extended range of the plastic deformation. In order to obtain the material strain-stress relationship in the extended range of the deformation, different work-hardening laws, including Ludwik law (Ludwick, 1922), Swift law (Swift, 1952) and Voce law (Voce, 1955), were fitted against the experimental stress-strain data, as shown in Figure 13(a). The optimized parameters for the hardening laws are presented in Table 3. Corresponding root sum square (RSS) of the errors between the predictions and experimental data were calculated. By comparison, it was shown that the prediction obtained by the Voce law was the closest to the experimental data and the trend so that it was used in the FE models to describe the plastic stress-strain curve in FE modelling of this study, as shown in Figure 13(b).

Table 3 Hardening laws and corresponding fitted values of the parameters for material AA5251-H22

Hardening Laws	AA5251-H22	RSS
Ludwik	$\sigma = 142.67 + 306.22 * \varepsilon_p^{0.51}$	18.89
Swift	$\sigma = 380.67 * (0.016 + \varepsilon_p)^{0.22}$	16.71
Voce	$\sigma = 153.11 + 100.67 * (1 - e^{-16.91\varepsilon_p})$	8.45

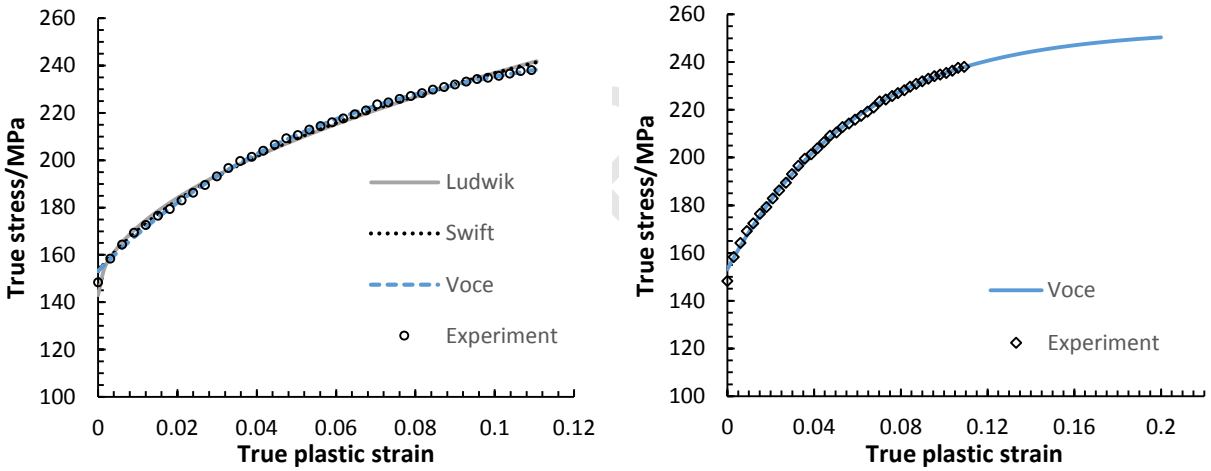

(a) (b)

Figure 13 Flow stress curve fitting for AA5251-H22: (a) comparison between different hardening laws and the experimental data; (b) extended flow stress curve predicted by the Voce law

Element type C3D8R was used for specimen in the FE modelling. According to the mesh convergence analysis results, the element size of 0.5mm was used in the central area of the specimen while the arms of the specimen were meshed as 2mm in element size, from which the displacement-force curves obtained from the experiment and the simulation were converged. Five layers of elements were used in the specimen thickness direction in order to observe the effect of bending and compression on the deformation behaviour. Meshing of the specimen is shown in Figure 14(a).

All rollers in the FE model of the TCBC test were defined as rigid bodies and their movements were controlled by the displacement boundary conditions. The specimen was fixed on one end while was stretched on the other end at a tensile speed of 2.4mm/min. The bending roller and the

compression roller moved together at a speed of 1.5mm/s. The compression was applied by an axial connector mechanism supporting the compression roller with a preload of 600N. The bending depth was defined as 9mm. To reduce the computational time, only half of the specimen was modelled by applying the axisymmetric boundary condition, as shown in Figure 14(a). Local coordinate systems were established on every single element in order to obtain stress components in the directions normal to the element surfaces after deformation. As a comparison, another FE model of TCB test, without applying compression force, was also established in which all other parameters were kept the same.

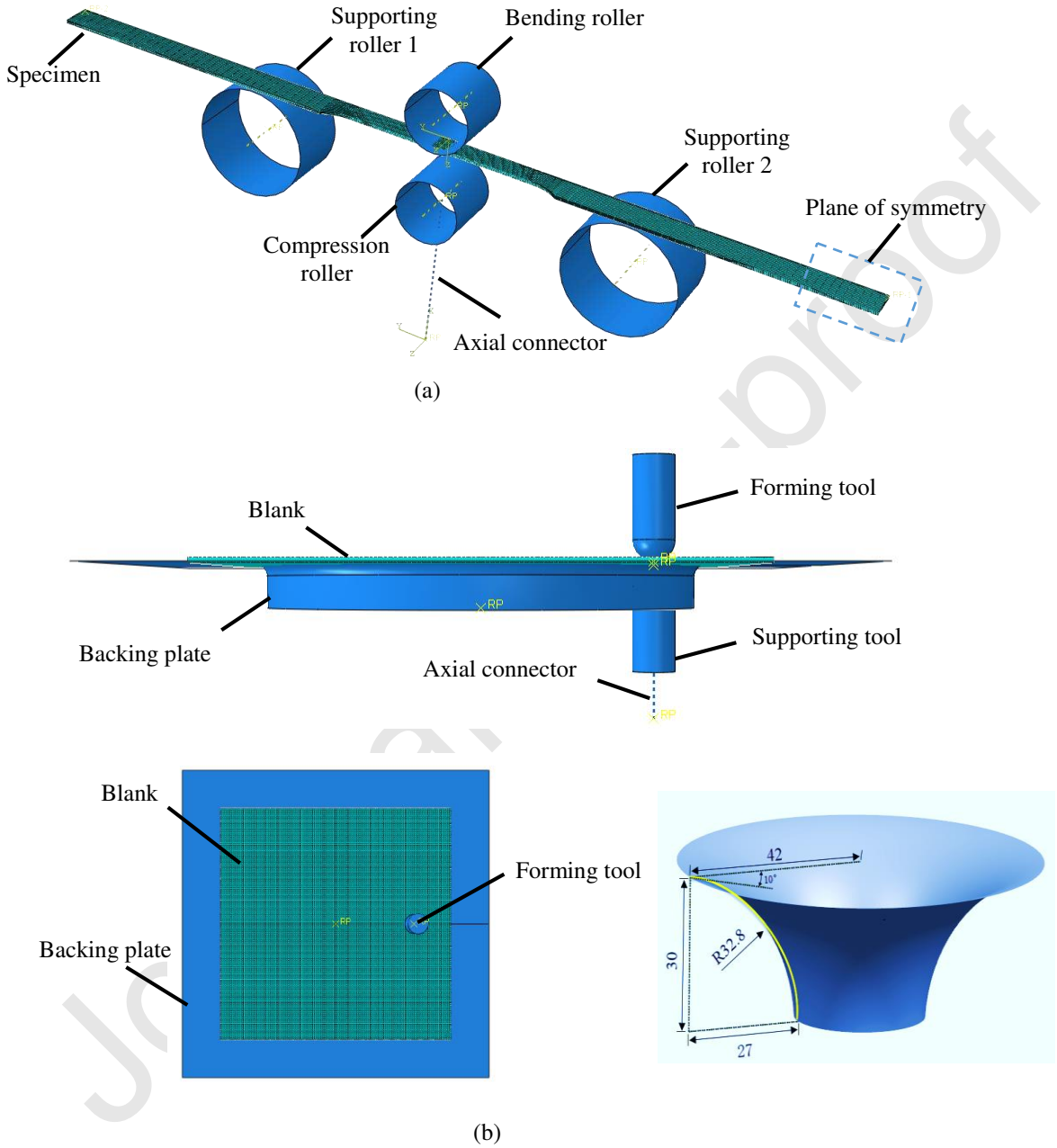

Figure 14 FE models: (a) TCBC test; (b) DSIF

In order to characterize the material deformation in DSIF process and to demonstrate the similarity between DSIF process and the proposed TCBC test, a FE model of DSIF process was also developed, as shown in Figure 14(b). The DSIF FE model can also be used for SPIF modelling by setting the compression as zero in the model. The blank with dimensions of 150×150×1mm was placed on the backing plate to ensure the stiffness of the structure and accuracy of formed

geometry. The forming tool and the supporting tool were positioned against each other on each side of the blank. The geometry to be deformed was a parabolic cone with an opening radius of 42mm, as shown in Figure 14(b). The movement of the tools followed a spiral toolpath with a vertical step of 0.3mm. The tools moved at a constant linear speed of 1800mm/min. Similar with the TCBC model, the compressive force of the supporting tool was also provided by the axial connector mechanism, the preload was 200N. Coulomb friction law was applied and the friction coefficient was set to be 0.1. The tools and the backing plate were defined to be rigid. Solid element type C3D8R was used in the meshing of the blank. The mesh size of the blank was 0.5mm in the sheet surface while five layers of element were used in the thickness direction.

5.2 FE modelling results

5.2.1 Localized material deformation

Equivalent plastic strain history of elements for TCBC and TCB tests, SPIF and DSIF processes were extracted from the FE modelling results, as shown in Figure 15 (a) and (b). It was obvious that in all four modelled tests and ISF processes, the material plastic deformation only occurred periodically when the tool(s) were in contact with the sheet. When the tool(s) moved away from the contact locations, the strains kept almost unchanged periodically. Stair-like evolution of the equivalent plastic strains indicated obvious characteristics of localised material plastic deformation in all four FE models simulating TCBC and TCB tests, and SPIF and DSIF processes.

5.2.2 Comparison between ISF and TCBC tests

Strain components of the elements in each thickness layer of the specimen were extracted from the four FE models, from which the strain paths were plotted, as shown in Figure 16(a) and (b). The non-linear strain paths reflected the effect of cyclic loading on the material deformation. For TCBC and TCB tests, the introduction of the compressive force reduced the material deformation in the lateral direction when elongations of the specimens in the longitudinal direction were the same. The difference between the strain paths obtained from the DSIF and SPIF processes was less obvious than that between the TCBC and TCB tests. The difference could be caused by two factors. Firstly, geometric constrains between the tests and the processes was different. In the TCBC and TCB tests, the material was under near plane stress condition. However, in the ISF processes, the material was confirmed to be under a strain state between plane strain and equi-biaxial tension. Secondly, how the tension was applied onto the material was different. In the TCBC and TCB tests, the tension was applied by the continuous stretching force from the clamp. By comparison, in the ISF processes, the sheet blank was only clamped on the outer edges, once the tool(s) moved away from the material, the tension applied on that area would be partially released due to the loss of constraint. As a result, the strain paths obtained from the TCBC and TCB tests were different from the ISF processes.

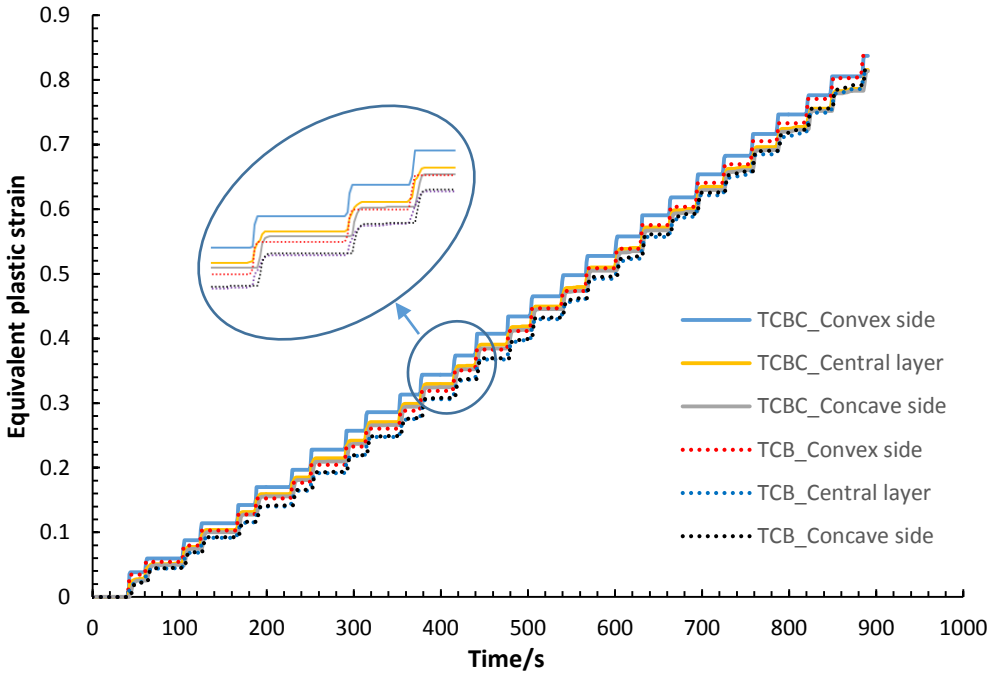

(a)

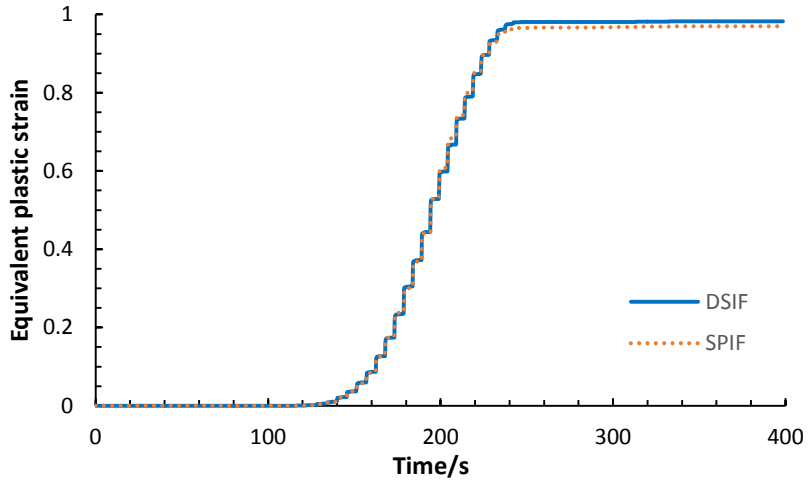

(b)

Figure 15 Equivalent plastic strain evolution of elements in FE modelling: (a) TCBC and TCB tests; (b) DSIF and SPIF processes

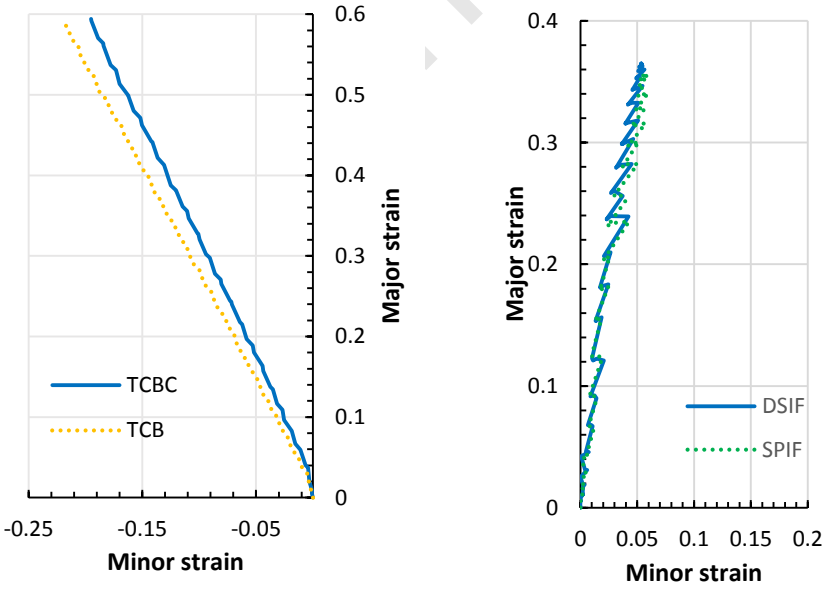

(a) (b)

Figure 16 Strain paths of elements in FE modelling of: (a) TCBC and TCB tests; (b) DSIF and SPIF processes

5.2.2 Effects of bending, tension and compression on the TCBC tests

Bending and tension effects were observed in both TCBC and TCB tests. Equivalent plastic strains of three elements located on the convex surface, the middle surface and the concave surface of the sheet thickness were extracted from the FE models of the TCBC and TCB tests. As shown in Figure 15(a), the elements in different layers in thickness direction showed different degrees of plastic deformation, which suggested the existence of bending effect in the thickness direction as illustrated in Figure 12. However, different from the pure bending effect, in which the deformation in the central layer should be under the smallest deformation, in the TCBC and TCB tests, the elements in the convex side of the specimen showed the largest plastic deformation. The central layers had the second largest plastic strain and the concave side elements had the smallest, which indicated a superimposed tension effect in addition to the bending effect. The bending effect could also be observed when comparing the distribution of the tensile stress in the longitudinal direction in the contact area across the thickness using the local coordinates, as shown in Figure 17. For both TCBC and TCB tests, the elements on the concave side within the contact area were under compression in the longitudinal direction, while on the convex side, they were under tension.

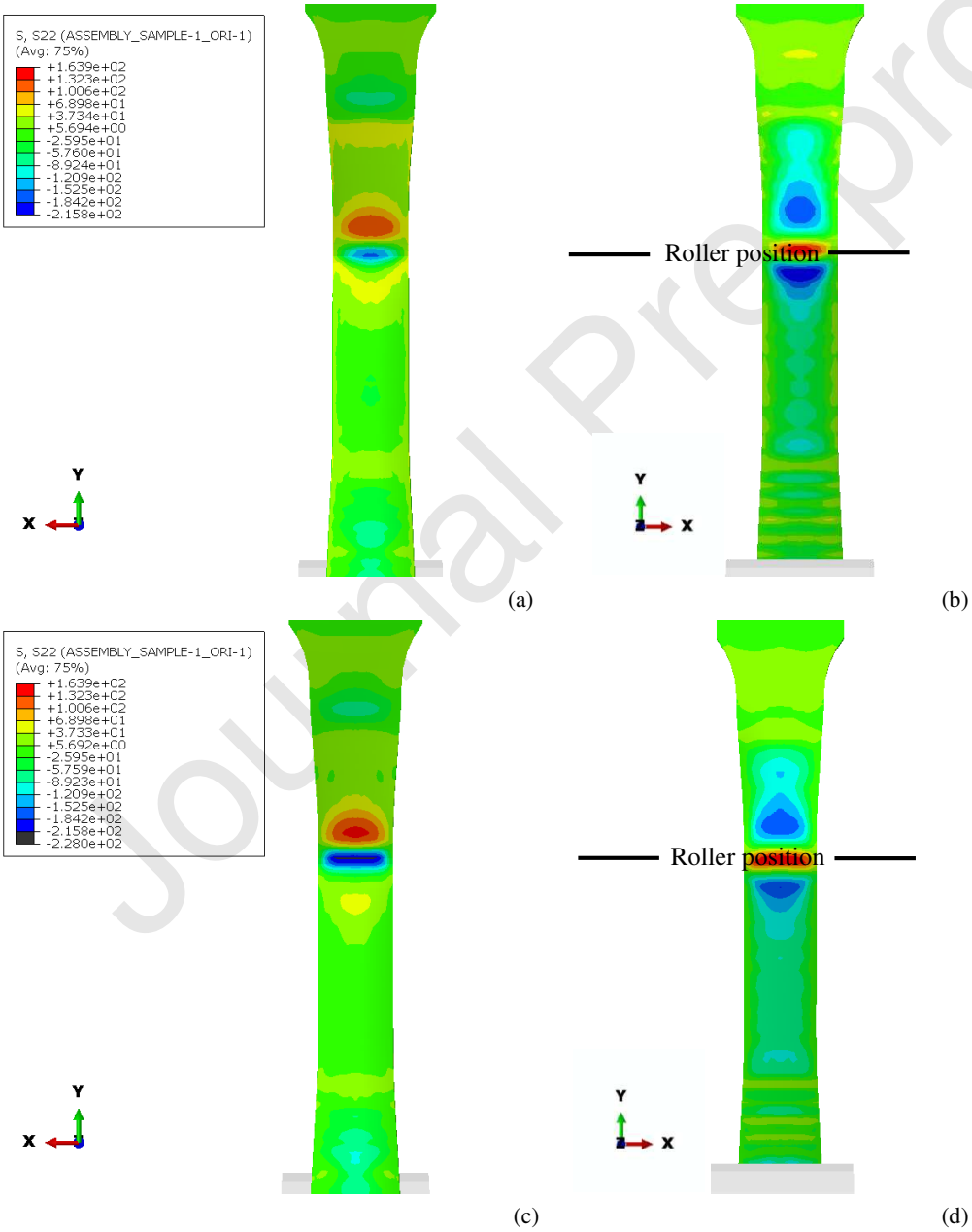

Figure 17 Stress distribution (MPa) in the longitudinal direction during the uniform material deformation stage: (a) TCBC test concave side; (b) TCBC test convex side; (c) TCB test concave side; (d) TCB test convex side

The introduction of the compression force improved the formability of the material. As shown in Figure 15(a), the equivalent plastic deformation of the elements in the TCBC test was obviously greater than those in the TCB test after the same loading cycles. Since the tensile speed was the same for both tests, a larger plastic deformation resulted in a thinner specimen thus a smaller tensile force needed to stretch the specimen to reach the same level of plastic deformation, as recorded in the experiment shown in Figure 9. Since the fracture in the TCBC test was caused by tension according to the experiment, less stretching effect led to larger plastic deformation before the occurrence of fracture.

In addition, the difference between the equivalent plastic strain of the elements on the concave side and the central layer was much larger in the TCBC test than that in the TCBC test, as shown in Figure 15(a). This indicated that the bending effect in the TCB test was much more obvious thus the neutral plane of the thickness was shifting from the central layer to the concave side of the specimen surface during the thinning process of the specimen. While in the TCBC test, the introduction of the compression force led a more homogeneous distribution of plastic deformation in the thickness direction thus less severe bending effect, creating a less obvious gradient of plastic deformation across the thickness direction.

6. Discussions

According to the experimental results, the material formability was further enhanced in TCBC test compared with that in the TCB test and the uniaxial tensile test, especially for material AA5251-H22. The FE modelling results confirmed the strong localised material plastic deformation in the TCBC test. Compared with that in the TCB test, the material tested under the TCBC reached higher plastic deformation with less tensile deformation, which led to higher maximum elongation of the specimen in the TCBC test. The stair-like accumulation of equivalent plastic deformation was observed in the FE modelling of TCBC and TCB tests. This was also observed in the developed FE models of SPIF and DISF processes to form a hyperbolic cone. The same observation was reported by Mirnia et al. (2018) in the FE simulation of SPIF process and by Smith et al. (2013) in the FE simulation of SPIF and ADSIF. The localised material deformation in the TCBC test confirmed that the newly developed TCBC test could be a reasonable representation of the DSIF process.

6.1 The effect of the investigated factors in the TCBC test

The introduction of the compression effect produced significant differences between the CBT test (Emmens and van den Boogaard, 2009) and the TCBC test. As observed from the experimental results in this study, the existence of compression force further improved the material formability in the TCBC test. The compression force was shown to be the most influential factor affecting the material formability in the experiment while the bending effect, which was the most influential factor in the CBT test, was comparatively weakened in the TCBC test, as also observed from the FE simulation results of TCBC and TCB tests in this study.

The material formability was further strengthened under the TCBC condition. The tensile force needed for yielding was smaller which further delayed the fracture caused by the tension effect. However, when the compressive force was increased beyond a certain limit, the fracture of the specimen occurred earlier. A similar phenomenon was also observed by Lu et al. (2015) when

performing the DSIF test, in which the maximum forming angle of the conic part started to decrease when the supporting pressure of the compression tool was increased to be higher than 600MPa. In their case, the earlier fracture was attributed to surface damage by the excessive pressure from the tools. However, in the TCBC test, the rollers were free to rotate around their own axis therefore no obvious surface damage caused by the tools was observed on either side of the specimen. A possible explanation could be when the compression force was larger enough, the material in the contact zone was prone to yield even with a small tensile force applied, according to the Tresca yielding criterion. Therefore, the fracture was more susceptible to the tension effect thus leading to early fracture.

The influence of the tensile speed was also different between the CBT and the TCBC tests. In the CBT test, the existence of tension was crucial to achieve the plastic deformation. If no tension exited, the whole process was degenerated to a pure bending test, thus a formability enhancement over the conventional forming processes was not feasible. By comparison, without the tension effect, the material formability enhancement in the TCBC process could still be achieved. In addition, without tension effect, the damage evolution was suppressed due to the compression dominated plastic deformation, which further maximised the material formability. The same concept of compression dominating deformation could be reflected in the process of the accumulative-DSIF (ADSIF) (Smith et al., 2013) where the tools moved outwards and upwards from the centre of the bottom of the toolpath. In ADSIF, the compression from the supporting tool reduced the tensile force needed for the plastic deformation. Furthermore, the reciprocating movements of the tool from inside to outside resulted in a free end of the ADSIF formed part which further reduced the tensile force.

By comparing CBT test and TCBC test results, it was obvious that the existence of superimposed compression onto the material deformation not only changed the relative significance of various deformation modes on the material but also introduced the interaction effect between these deformation modes. In the CBT test, the stretching speed and the bending depth were combined to produce the bending effect while in the TCBC test, as analysed in Section 4.1, the effect of stretching speed was significantly weakened due to the introduction of the compression effect. This showed that the effect of every single deformation mode could not be isolated in the analysis.

The selection of the variation ranges of the testing parameters to achieve the maximum material formability in the TCBC process depended on the material type. The reason was twofold. Firstly, different types of materials showed a different degree of sensitivity to the variations of the parameters tested in the experiment. In this study, material AA5251-H22 was obviously more sensitive to the parameters investigated and the variation ranges led to a significant material formability enhancement in the test. While AA6082-T6 only displayed a slight increase of the maximum elongation when the similar variation ranges of the parameters were used. Furthermore, the interaction between the process parameters made it very difficult to predict the trend of the formability enhancement when the parameters were varied; there was no general trend observed.

Based on the findings in the TCBC test, a guidance to maximize the material formability in the DSIF process could be proposed. A different level of the compression force may be required for a different material. The gradient of the toolpath in the vertical movement direction should be appropriate to avoid excessive tension effect in the meridional direction of the ISF formed part

when the forming tool deforming the material, this also should be considered when determining the vertical step of the toolpath.

6.2 Limitations of the current TCBC test method

Some limitations were observed in the current investigation of the TCBC tests in this study. In the experiments conducted, the variation ranges of the factors investigated were limited due to the limited capability of the current TCBC test rig design, especially for the material AA6082-T6. A greater variation range of the factors should be investigated in the future. For example, for both types of materials, the stroke speed presented a positive effect on the material formability but the degree of the influence tended to decrease while the stroke speed was increased. A new trend of the effect of the stroke speed on the material formability may emerge when the testing range of the parameter variations could be extended.

The shearing effect along the roller movement direction resulted from the friction between the tools and the specimen was neglected in the current TCBC test due to the fact that the magnitude of rolling friction between the rollers and the specimen surfaces was much smaller than sliding friction. If the rollers could be fixed to prevent self-rotation around their own axis, the friction-related shearing effect could be more obvious, and the magnitude of the frictional effect could be evaluated by using different types of lubricants. The magnitude of bending effect in the TCBC test could be affected by bending depth, roller radius and material thickness. In the current test, only bending depth and material thickness were varied while the bending roller radius was kept constant as 10mm. Further experiments using rollers with different radii could be conducted.

The results obtained from the Taguchi Design of the Experiments with four factors and the third stage experiments demonstrated the interactive effect between the key factors tested. However, the interactive effect of all important parameters can only be appropriately investigated by introducing the interaction factors into the design of the experiments. It cannot be analysed using the current experimental design of four factors, more factors representing interactive effects between the current four factors need to be considered in the test design and more sets of experiment to be conducted.

The FE results revealed that although the TCBC test created a localised deformation in the material, the strain paths were still different from those obtained from the ISF processes due to the difference in the loading conditions and geometrical constraints of the sheet material. To achieve a better simplified representation of the ISF processes, the geometrical constrain in the ISF processes should be taken into consideration in developing simplified testing methods in the future.

In DSIF process, the relative position of the two tools was reported to be an important factor affecting the material formability in DSIF since it changed the contact conditions which led to different strain and stress distributions in the specimen (Lu et al., 2015). Using the current TCBC test rig, the compression roller was positioned to touch the centre of the bending area of the specimen, created by the bending roller. If the compression roller could be shifted to be away from the centre of the bending area, the relative position of the two tools in the DSIF process, as shown in Figure 1(b), could be evaluated, subsequently its influence on the formability could be investigated.

7. Conclusions

A new testing method, the tension under bending and compression (TCBC) test, is developed in this study to investigate the effect of various deformation modes on the material formability enhancement in DSIF. Based on the results obtained from the theoretical analysis, experimental testing and the FE modelling, the following conclusions can be made:

(1) Among the four deformation modes, the compression was the most significant factor affecting the material formability in the TCBC test for two materials tested, AA5251-H22 and AA6082-T6;

(2) Bending in general was beneficial to the material formability improvement in the TCBC test, however its effect can be influenced by the magnitude of compression loading applied;

(3) Different materials showed different sensitivity to the variation of the tested parameters when investigating the material formability enhancement, in this study, material AA5251-H22 was far more sensitive than AA6082-T6;

(4) Localised deformation in the contact zone was clearly evident in both the TCBC and TCB tests, which was further strengthened in the TCBC test when an appropriate range of the compression was applied, reducing the tensile force required for initiating plastic deformation thus delaying the occurrence of fracture;

(5) To maximize the material formability in the DSIF process, the magnitudes of the compression and the vertical increment of the tool path should be optimised when forming different materials and geometries to avoid excessive tensile force and early material fracture.

(6) The TCBC test method demonstrated its potential to be a simplified method in testing the material deformation and investigating the fracture mechanisms for DSIF to replace the current test method using the DSIF process itself for material formability studies.

8. Acknowledgement

The authors acknowledge Dr. Bin Lu's contribution to the development of the TCBC test method and test rig as part of EU FP7 Marie Curie Actions International Fellowship: FLEXFORM Project (FP7-PEOPLE-2013 IIF 628055). The authors are also grateful to senior mechanical technician David Webster for his support to the development and manufacturing of the TCBC test rig. The first author would like to acknowledge the PhD scholarship received from the Faculty of Engineering, The University of Sheffield to support this research.

9. References

Ai, S., Long, H., 2019. A review on material fracture mechanism in incremental sheet forming. International Journal of Advanced Manufacturing Technology. https://doi.org/10.1007/s00170-019-03682-6.

Ai, S., Lu, B., Chen, J., Long, H., Ou, H., 2017. Evaluation of deformation stability and fracture mechanism in incremental sheet forming. International Journal of Mechanical Sciences 124, 174-184.

Ai, S., Lu, B., Long, H., 2017. An analytical study of new material test method for tension under bending and compression in double side incremental forming. Procedia Engineering 207, 1982-1987.

ASTM American Society for Testing and Materials, 2009. Standard test methods for tension testing of metallic materials. ASTM international.

Behera, A.K., de Sousa, R.A., Ingarao, G., Oleksik, V., 2017. Single point incremental forming: An assessment of the progress and technology trends from 2005 to 2015. Journal of Manufacturing Processes 27, 37-62.

Duflou, J., Callebaut, B., Verbert, J., De Baerdemaeker, H., 2008. Improved SPIF performance through dynamic local heating. International Journal of Machine Tools and Manufacture 48, 543-549.

Duflou, J.R., Habraken, A.-M., Cao, J., Malhotra, R., Bambach, M., Adams, D., Vanhove, H., Mohammadi, A., Jeswiet, J., 2017. Single point incremental forming: state-of-the-art and prospects. International Journal of Material Forming, 1-31.

Emmens, W.C., Sebastiani, G., Van den Boogaard, A., 2010. The technology of incremental sheet forming—a brief review of the history. Journal of Materials Processing Technology 210, 981-997.

Emmens, W.C., van den Boogaard, A.H., 2009. Incremental forming by continuous bending under tension—An experimental investigation. Journal of materials processing technology 209, 5456-5463.

Emmens, W.C., van den Boogaard, A.H., 2009. An overview of stabilizing deformation mechanisms in incremental sheet forming. Journal of Materials Processing Technology 209, 3688-3695.

Eyckens, P., Belkassem, B., Henrard, C., Gu, J., Sol, H., Habraken, A.M., Duflou, J.R., Van Bael, A., Van Houtte, P., 2011. Strain evolution in the single point incremental forming process: digital image correlation measurement and finite element prediction. International journal of material forming 4, 55-71.

Eyckens, P., Van Bael, A., Van Houtte, P., 2009. Marciniak–Kuczynski type modelling of the effect of through-thickness shear on the forming limits of sheet metal. International Journal of Plasticity 25, 2249-2268.

Fang, Y., Lu, B., Chen, J., Xu, D., Ou, H., 2014. Analytical and experimental investigations on deformation mechanism and fracture behavior in single point incremental forming. Journal of Materials Processing Technology 214, 1503-1515.

Fratini, L., Ambrogio, G., Di Lorenzo, R., Filice, L., Micari, F., 2004. Influence of mechanical properties of the sheet material on formability in single point incremental forming. CIRP Annals-Manufacturing Technology 53, 207-210.

Hussain, G., Gao, L., Zhang, Z., 2008. Formability evaluation of a pure titanium sheet in the cold incremental forming process. The International Journal of Advanced Manufacturing Technology 37, 920-926.

Jackson, K., Allwood, J., 2009. The mechanics of incremental sheet forming. Journal of materials processing technology 209, 1158-1174.

Jeswiet, J., Hagan, E., 2001. Rapid prototyping of a headlight with sheet metal. Canadian Institute of Mining, Metallurgy and Petroleum(Canada), 109-114.

Jeswiet, J., Micari, F., Hirt, G., Bramley, A., Duflou, J., Allwood, J., 2005. Asymmetric single point incremental forming of sheet metal. CIRP Annals-Manufacturing Technology 54, 88-114.

Kim, Y., Park, J., 2002. Effect of process parameters on formability in incremental forming of sheet metal. Journal of materials processing technology 130, 42-46.

Liu, R., Lu, B., Xu, D., Chen, J., Chen, F., Ou, H., Long, H., 2016. Development of novel tools for electricity-assisted incremental sheet forming of titanium alloy. The International Journal of Advanced Manufacturing Technology 85, 1137-1144.

Lu, B., Fang, Y., Xu, D., Chen, J., Ai, S., Long, H., Ou, H., Cao, J., 2015. Investigation of material deformation mechanism in double side incremental sheet forming. International Journal of Machine Tools and Manufacture 93, 37-48.

Lu, B., Fang, Y., Xu, D., Chen, J., Ou, H., Moser, N., Cao, J., 2014. Mechanism investigation of friction-related effects in single point incremental forming using a developed oblique roller-ball tool. International Journal of Machine Tools and Manufacture 85, 14-29.

Lu, B., Ou, H., Shi, S., Long, H., Chen, J., 2016. Titanium based cranial reconstruction using incremental sheet forming. International Journal of Material Forming 9, 361-370.

Ludwick, P., 1922. 'Uber den Einfluss der Deformationsgeschwindigkeit bei bleibenden Deformationen mit besonderer Berucksichtigung der Nachwirkungserscheinungen. Phys. Z 10, 411-417.

Maqbool, F. and M. Bambach, 2018. Dominant deformation mechanisms in single point incremental forming (SPIF) and their effect on geometrical accuracy. International Journal of Mechanical Sciences 136, 279-292.

Martins, P., Bay, N., Skjødt, M., Silva, M., 2008. Theory of single point incremental forming. CIRP Annals-Manufacturing Technology 57, 247-252.

Minitab, USA, 2014. MINITAB release 17: statistical software for windows.

Mirnia, M.J., Vahdani, M., Shamsari, M., 2018. Ductile damage and deformation mechanics in multistage single point incremental forming. International Journal of Mechanical Sciences 136, 396-412.

Morales, D., Martinez, A., Vallellano, C., Garcia-Lomas, F., 2009. Bending effect in the failure of stretch-bend metal sheets. International Journal of Material Forming 2, 813.

Narasimhan, N., Lovell, M., 1999. Predicting springback in sheet metal forming: an explicit to implicit sequential solution procedure. Finite elements in analysis and design 33, 29-42.

Rodríguez, P.P., 2006. Incremental sheet forming Industrial applications–, International Seminar on Novel Sheet Metal Forming Technologies.

Schrader, G., Elshennawy, A.K., 2014. Manufacturing Processes and Materials. Society of Manufacturing Engineers.

Silva, M., Skjødt, M., Martins, P.A., Bay, N., 2008. Revisiting the fundamentals of single point incremental forming by means of membrane analysis. International Journal of Machine Tools and Manufacture 48, 73-83.

Smith, J., Malhotra, R., Liu, W., Cao, J., 2013. Deformation mechanics in single-point and accumulative double-sided incremental forming. The International Journal of Advanced Manufacturing Technology 69, 1185-1201.

Swift, H.W., 1952. Plastic instability under plane stress. Journal of the Mechanics and Physics of Solids 1, 1-18.

Voce, E., 1955. A practical strain hardening function. Metallurgia 51, 219-226.